AGU PUBLICATIONS

Geochemistry, Geophysics, Geosystems

RESEARCH ARTICLE
10.1002/2015GC005954

Key Points:
- A modern altitude proxy is proposed for the Atacama Desert based on $^{87}Sr/^{86}Sr$ of Holocene surficial accumulations of gypsum
- The proxy's bimodal, single-threshold nature derives from the dynamics of marine aerosols

Supporting Information:
- Supporting Information S1
- Table S1

Correspondence to:
N. J. Cosentino,
njc58@cornell.edu

Citation:
Cosentino, N. J., T. E. Jordan, L. A. Derry, and J. P. Morgan (2015), $^{87}Sr/^{86}Sr$ in recent accumulations of calcium sulfate on landscapes of hyperarid settings: A bimodal altitudinal dependence for northern Chile (19.5°S–21.5°S), *Geochem. Geophys. Geosyst.*, *16*, 4311–4328, doi:10.1002/2015GC005954.

Received 17 JUN 2015
Accepted 23 NOV 2015
Accepted article online 26 NOV 2015
Published online 29 DEC 2015

$^{87}Sr/^{86}Sr$ in recent accumulations of calcium sulfate on landscapes of hyperarid settings: A bimodal altitudinal dependence for northern Chile (19.5°S–21.5°S)

N. J. Cosentino[1], T. E. Jordan[1], L. A. Derry[1], and J. P. Morgan[2]

[1]Department of Earth and Atmospheric Sciences, Cornell University, New York, USA, [2]Department of Earth Sciences, Royal Holloway, University of London, London, UK

Abstract An elevation-dependent relationship of the $^{87}Sr/^{86}Sr$ ratio of Holocene surface accumulations of sulfate salts is demonstrated for a continental margin hyperarid setting. In the Atacama Desert of northern Chile, gypsum and anhydrite of multiple origins exist widely on superficial materials that originated during the last 10,000 years. An important source of calcium sulfate is from offshore-generated stratocumulus clouds that are advected onto the continent, where they generate fog that transfers water droplets to the ground surface which, upon evaporation, leaves calcium sulfate crystals. Meteorological measurements of the cloud base and top altitudes average ~400 m and ~1100 m above sea level (masl), respectively. The seawater ratio of $^{87}Sr/^{86}Sr$ (0.70917) is distinctively higher than that reported for weathered mean Andean rock (less than 0.70750). Samples of 28 modern surface salt accumulations for locations between 200 and 2950 masl and between ~19°30′ and ~21°30′S verify that $^{87}Sr/^{86}Sr$ varies as a function of site altitude. Sites below 1075 masl and above 225 masl display calcium sulfate $^{87}Sr/^{86}Sr$ of mean value 0.70807 ± 0.00004, while the ratio outside this altitudinal domain is 0.70746 ± 0.00010. Thus, the $^{87}Sr/^{86}Sr$ ratio of Holocene salt accumulations differentiates two altitudinal domains.

1. Introduction

Quantification of uplift of a continental surface relative to sea level is challenging [*Rowley and Garzione*, 2007] and is a topic of active research in the Andes [*Gregory-Wodzicki*, 2000; *Schlunegger et al*., 2006; *Garzione et al*., 2008; *Farías et al*., 2008; *Jordan et al*., 2010; *Insel et al*., 2012]. Quantified studies of topographic uplift of the continental part of a fore-arc system have been generally limited to documenting the temporal history of shoreline positions, such as along western South America [*Saillard et al*., 2009, 2011; *Bourgois*, 2010], in Costa Rica and Panama [*Sak et al*., 2009; *Morell et al*., 2011] and in southern Italy [*Ferranti et al*., 2007].

The South America, Nazca plate fore-arc system in northern Chile hosts the hyperarid Atacama Desert. In a hyperarid setting, traditional $\delta^{13}C$ and $\delta^{18}O$ stable isotope paleoaltimetric methods are generally not suitable due to the impacts of evaporation on isotopic ratios. Instead, saline surface materials are widely available. *Rech et al*. [2003] examined soil-forming processes in the Atacama Desert and revealed an apparent relationship between Sr isotopic composition of calcium sulfate soils and altitude, whose potential utility for paleoaltimetry has not been probed.

Before any paleoaltitude investigation would be justified, a much more extensive analysis is needed of the relationships between $^{87}Sr/^{86}Sr$ of surficial materials, the elevations of the sites in the landscape at which those saline materials occur, and other factors that may influence the $^{87}Sr/^{86}Sr$ of these materials. Here we document and analyze the relationship between the Sr isotope signature of geologically recent salt accumulations and their altitude of formation or deposition within the modern fore-arc system of the Atacama Desert, between 19.5°S and 21.5°S.

2. Physical and Chemical Bases for the Proxy

2.1. Controls on Climate of the Atacama Desert

The Atacama Desert is among the driest places on Earth. Located in northern Chile and southernmost Peru between 17° and 27°S, it is bounded to the east by the western front ranges of the Andes Mountains

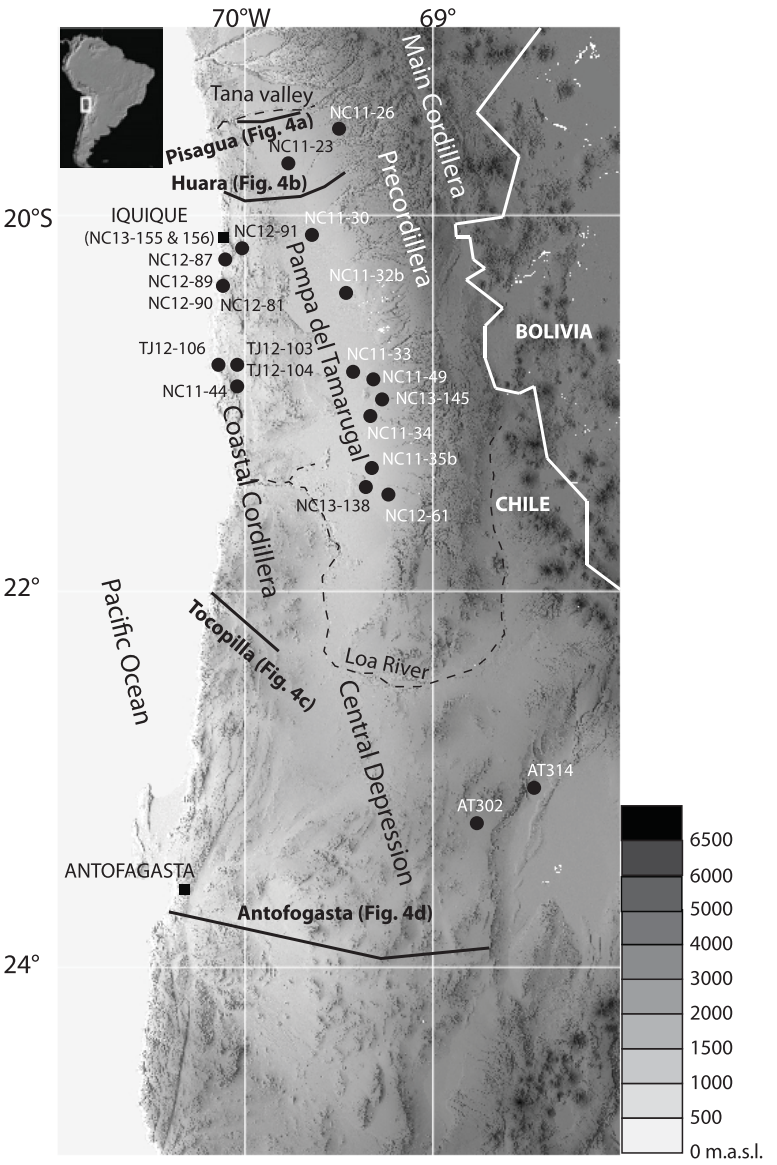

Figure 1. Main morphotectonic units of the inland fore arc of the Nazca-South America plate system (see text for discussion). Topography is shown as a grey scale on the map, with shading accomplished by light coming from the west in order to better show topographic features. Black lines show the locations of the sample transects, of which the Tocopilla and Antofagasta transects were sampled by *Rech et al*. [2003]. Black dots are single sampling sites, of which AT302 and AT314 were sampled by *Rech et al*. [2003].

(western Precordillera) and to the west by the Pacific Ocean (Figure 1). In this region, the potential evapotranspiration (PET) is between 1 and 2 mm d^{-1} [*Mintz and Walker*, 1992]. According to *United Nations Environment Program/Global Resource Information Database* [1991], for this PET, the climate is classified as "hyperarid" wherever the mean annual precipitation is below 20–40 mm yr^{-1}, a condition met widely below 3000 masl altitude [*Houston and Hartley*, 2003]. Three atmospheric and oceanic phenomena contribute to the arid conditions: the large-scale atmospheric subtropical subsidence due to the presence of the South Pacific High [e.g., *Rodwell and Hoskins*, 2001], the local atmospheric subsidence related to easterly flow over the Andes [e.g., *Houston and Hartley*, 2003], and the cold sea surface temperatures (SST) near the land, which are maintained by upwelling of cold Pacific deep waters near the coast [*Takahashi and Battisti*, 2007]. This upwelling is a response to offshore Ekman transport of oceanic water associated with equator-ward alongshore surface winds, which drive the eastern boundary current along the coasts of Chile and Peru. These conditions combine to greatly reduce precipitation over the area [*Wang et al*., 2004; *Takahashi and*

Battisti, 2007]: southeast Pacific westerly moist air masses are blocked by the high-pressure zone offshore; the Andes create a rain shadow; atmospheric convection is suppressed by the cold SST and the subtropical subsidence, producing a persistent temperature inversion. A result of these conditions is a persistent stratocumulus cloud deck produced offshore and advected inland by southwesterly winds, where they produce fog [*Cereceda et al*., 2002]. Due to the low-altitude atmospheric temperature inversion, the stratocumuli clouds are trapped at low-altitudes. It is this combination of an extreme lack of precipitation and the widespread presence of stratocumulus cloud decks and fog that make the Atacama such a unique desert.

2.2. Chilean Fore-Arc Physiography and Geology

The major landforms of the study area (Figure 1) are a narrow, 0–3.5 km wide coastal platform, an angle-of-repose escarpment (Coastal Escarpment) facing the Pacific Ocean, across which altitudes rise to 500–1200 masl, a 30–60 km wide mountain belt (Coastal Cordillera) with elevations generally $<$2000 masl, and a 50–75 km wide valley inland of the coastal range (Central Depression) at $\sim$1000–2500 masl. The study area is bounded to the east by the western foothills of the Andes (western Andean slope and Precordillera). Geologically, the Coastal Cordillera is composed predominantly of Jurassic volcanic rocks and Jurassic-Early Cretaceous dioritic to granodioritic plutonic rocks [*SERNAGEOMIN*, 2003; *Vásquez and Sepúlveda*, 2013]. A series of fore-arc sedimentary basins comprise the Central Depression, filled with strata of Oligocene to recent age [*Hoke et al*., 2007]. In the study area, the basin is known as the Pampa del Tamarugal. In general, the Coastal Cordillera and Central Depression constitute a gently rolling series of hills and a plain. Between 19.53°S and 21.43°S, the Pampa del Tamarugal is internally drained, but to the north a series of deep canyons traverse the fore arc to reach the Pacific Ocean, of which the southernmost is the Tana valley. Farther south, the Loa River flows parallel to the Central Depression and then drains to the Pacific through a deep canyon (Figure 1). Locally, salars (salt pans) cover broad areas near the boundary between the Pampa del Tamarugal and the Coastal Cordillera and occur within the Coastal Cordillera.

2.3. Superficial Sulfate Deposits of the Atacama Desert

Macroscopic superficial salt minerals occur widely in the Atacama, in landscape positions as variable as the Coastal Escarpment, the Coastal Cordillera mountains and valleys, the salt pans of both the Coastal Cordillera and the Central Depression, alluvial fans and piedmont slopes of the Central Depression, and within incised abandoned channels and valleys that traverse the Central Depression. Although many Atacama surfaces are formed of a composite of materials of uncertain antiquity [*Jordan et al*., 2014], we focus on parts of the landscape that formed since 10,000 years ago. That time range is selected because it is the time span since the last regionally documented extended period of wetter climate within the Central Depression [*Nester et al*., 2007; *Quade et al*., 2008; *Gayó et al*., 2012]. Within the Coastal Cordillera, *Vargas and Ortlieb* [1998] described a series of landscape stages corresponding to climate variations of the late Pleistocene and Holocene. *Marquet et al*. [2012] argued that archeological remains in the Coastal Cordillera are suggestive of an additional time of wetter environmental conditions $\sim$7000 to $\sim$4200 years ago. *Herrera and Custodio* [2014] presented evidence of sufficient precipitation along the western flank of the Coastal Cordillera $\sim$5000–3000 years ago to recharge local aquifers. Together, these results imply that for some landscape positions the maximum age for persistent hyperarid conditions and for what we treat as "superficial" gypsum is less than $\sim$4000 years.

The materials that host the superficial gypsum and anhydrite include gravel on the beds of fluvial channels, eolian sands, human relicts and, on the Coastal Escarpment only, bedrock and colluvium. A high rate of development of gypsum and anhydrite under modern conditions is clearly demonstrated by two reported cases of entombment in calcium sulfates of newspapers from the early twentieth century within anthropogenically disturbed parts of the landscape surface, both in locations subjected often to fog [*Searl and Rankin*, 1993; D. Burr and R. Jacobsen, personal communication, 2014].

Superficial gypsum and anhydrite crystals that are intermixed with fine-grained siliciclastics are commonly white to tan powdery materials and occur in several morphologies [*Jordan et al*., 2014]. One variety forms crusts $<$2 mm thick on the base of pebbles, cobbles, and boulders that lie on the landscape surface. These gypsum/anhydrite crusts are not laterally continuous, but rather are isolated under single clasts (Figure 2a). Nevertheless, these crystals act as incipient cement among grains of sand that comprise the fine-grained matrix surrounding the bases of those cobbles, over a distance from the cobbles of $<$10 mm. *Azúa-Bustos*

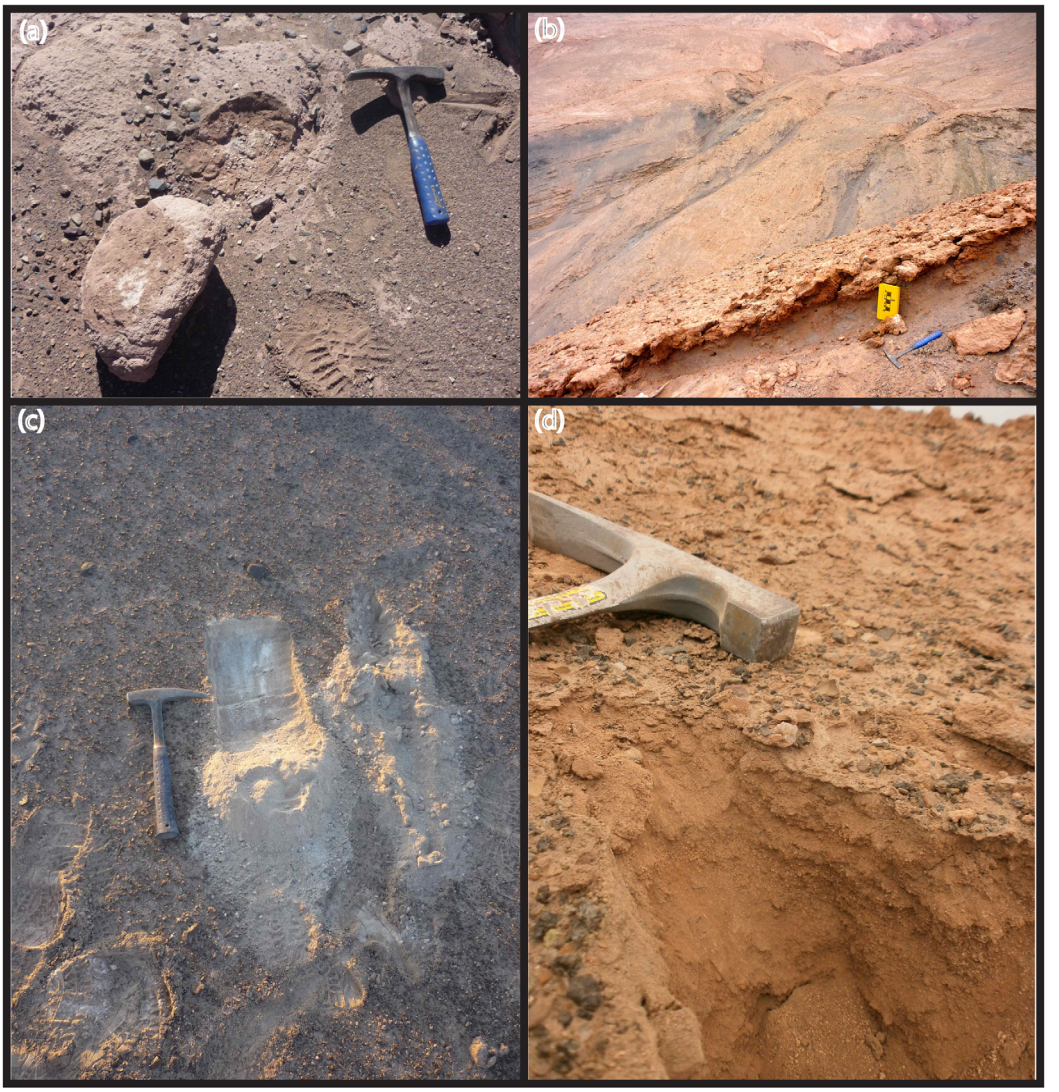

Figure 2. (a) Surficial white powdery intermixture of siliciclastic and salt material loosely attached to the bottom of pebbles, cobbles, and boulders (upside-down boulder in the image); (b) widespread 10–20 cm-thick surficial tan/rusty brown crust composed of gypsum and anhydrite and with a low clast density, and usually developed over a bedrock parent material; (c) 2 cm-thick surficial light tan/white laterally continuous powdery material (chusca) below a mm-scale lag gravel; and (d) surficial mm-scale gypsum-rich crust.

et al. [2011] showed that the efficiency of capture of water from fog increases with clast particle size, a fact consistent with the occurrence of gypsum/anhydrite crystals mostly under clasts with diameter >5 cm.

A second variety of superficial sulfates is also powdery but occurs as a laterally continuous layer overlying alluvium or salt pan accumulations, where formation of the underlying material is attributed to the Holocene [e.g., *Vásquez and Sepúlveda*, 2013]. These superficial dust accumulations are commonly several centimeters to tens of centimeters thick (Figure 2c). In some parts of the landscape, they form continuous horizons over many square kilometer areas, but they also are heavily pock marked by many-meter-wide deflation pits.

A third type of superficial sulfate occurs as mm-scale laterally continuous calcium sulfate-rich soft crusts (Figure 2d), which weakly cement siliciclastic detritus. These crusts lie at the surface-air interface and follow the relief of the underlying rock surface or soil surface. They can be found on surfaces of the Coastal Escarpment, the Coastal Cordillera, and the Central Depression.

A fourth class of superficial sulfate occurs also along the Coastal Escarpment, where the near-surface geological materials are a mixture of bedrock, talus, eolian sand dunes and sheets, debris flows, and colluvium

[*Orellana Cortés*, 2010]. The sulfate cover material consists of a widespread crust typically 10–20 cm thick, tan to rusty brown in color, and composed mostly of salts with a low clast density (Figure 2b). This thick gypsum/anhydrite crust is usually developed over a bedrock parent material. The steep coastal scarps are subjected to mega-earthquakes on a millennial time scale, and strong earthquakes on a century time scale [e.g., *Comte and Pardo*, 1991]. Moderate-sized earthquakes in modern times have provoked widespread downslope movement of both bedrock and surficial material [*Marquardt et al*., 2006], which would lead to disaggregation of a surficial gypsic crust. Thus, we interpret the third and fourth categories of superficial sulfate crusts of the Coastal Escarpment to be less than 10,000 years in age.

The salts comprising these cobble-bottom powders, thick dust accumulations, and superficial crusts are likely polygenetic. Some of the calcium sulfate crystals are recently formed (e.g., by recent wet deposition from marine aerosols or from evaporation of water at the edge of an ephemeral pond), but some of the crystals may have formed long ago and then later were physically translated by wind or water. For example, the modern winds may first erode the gypsum deposits of a Pleistocene-age salar, and then transfer it to a new landscape location. Another likely example is that wind and water erode gypsum and anhydrite from Miocene and Pliocene gypsic relict soils and integrate those pre-Holocene materials into the Holocene superficial calcium sulfate population. Although it may be polygenetic, the gypsum and anhydrite dust is a part of the Holocene surface system.

For this study, the target samples are calcium sulfates that are representative of salt accumulations that were created or reworked within the Holocene climate regime. It may appear that it would be challenging to distinguish a polygenetic Holocene salt deposit from a more ancient gypsum-rich soil, since they are compositionally the same. However, the pre-Holocene soils have a moderately to well-developed set of diagnostic pedogenic features (reviewed recently by *Jordan et al*. [2014]). If a soil cross section is well exposed, the pre-Holocene soils can be readily distinguished from the Holocene powders and crusts described above. Materials sampled initially from locations where differentiation between Holocene and pre-Holocene sulfates was ambiguous were excluded from the final analysis.

2.4. Incursions of Marine-Sourced Fog Into the Continental Interior

Fog is a characteristic phenomenon in the northern Chile fore arc, especially during the austral winter season. By using GOES satellite images to study the spatial and temporal behavior of stratocumulus clouds and their associated fog events, *Cereceda et al*. [2002] and *Farías et al*. [2005a] show that two main types of fog impact the continental surface and can be distinguished by their formation process. Advective fog events are the most widespread and result from advection of South Pacific stratocumulus clouds onto the continent by southwesterly winds. Orographic fogs are more localized phenomena and form on the first windward slope facing the sea when incoming air masses ascend due to topographic obstacles and cool adiabatically, condensing water vapor [*Cereceda et al*., 2002].

Topography is a first-order control on the vertical structure and spatial distribution of advective fog, which contacts the Coastal Escarpment within an altitudinal band whose base and top are higher and lower than 400 and 1100 masl, respectively [*Cereceda et al*., 2002]. Both in Peru and Chile, fog thickness on any given day is between 300 and 400 m [*Espejo*, 2001; *Cereceda et al*., 1997; *Cereceda and Schemenauer*, 1998]. *Farías et al*. [2005a] studied the spatial and temporal evolution of an advective event that took place 4–5 August 2001, also using GOES satellite images. This advective fog event lasted ~21 h and had a latitudinal reach of approximately 200 km. Over a time span of a month (August 2001), the fog coverage was maximum on the Coastal Escarpment, intermediate along lowland topographic corridors connecting the escarpment with the Central Depression, and least within the Central Depression [*Farías et al*., 2005a]. The most eastward penetration of the fog is strongly correlated with the 1100 masl contour line. Based on that body of work, for the following discussion the *observational fog zone* is treated as the continental area with altitudes between 400 and 1100 masl.

2.5. Fog Water Chemistry

The water quality of coastal fog in northern Chile has been examined by *Schemenauer and Cereceda* [1992] for sites near 29°30″S and *Sträter et al*. [2010] at the Alto Patache fog oasis (20°49′S, 70°09′W). These studies reported chemistry of advective fog captured in traps, which are plastic strips through which persistent strong winds blow the water-laden air. The wind may also transport dust from nearby ground surfaces. Fog samples of events originating over the Pacific had pH value means of 4.99 (standard deviation 0.86) and

4.65 (standard deviation 0.89) [*Schemenauer and Cereceda*, 1992] and between 2.9 and 3.5 [*Sträter et al*., 2010]. Both studies report high ionic concentrations coming from sea salt. *Sträter et al*. [2010] further concluded that anthropogenic activity was to blame for the high concentrations of heavy metals and contributed to the low pH, specifically mineral processing facilities, ship traffic, and power plants. For Holocene fog water predating anthropogenic contributions, the pH was likely more similar to the ~4.5–5 conditions reported by *Schemenauer and Cereceda* [1992].

2.6. $^{87}Sr/^{86}Sr$ in Surficial Salt Deposits

Sr is known to substitute for Ca in many mineral phases, and since calcium sulfate minerals are abundant in our surficial deposits, Sr isotopes are ideal for investigating the primary source of Atacama salts and soils. *Rech et al*. [2003] pioneered this approach, documenting $^{87}Sr/^{86}Sr$ and $\delta^{34}S$ of soil gypsum/anhydrite along three ~E–W transects. They took advantage of the very different Sr isotope ratios of seawater and salts derived from the weathering of Andean rocks, or derived by weathering but recycled through salars, to identify the degree to which marine aerosol contributes to soil salt.

Modern seawater has a well-known $^{87}Sr/^{86}Sr$ value of 0.70916 ± 0.00002 [*Farrell et al*., 1995]. *Rech et al*. [2003] estimated the Sr isotopic ratio of typical Andean weathering products east of the Coastal Cordillera, using aquatic mollusks and tufa from streams in the western Andean slope, Andean lake salts, and salar salts both at the base of the Andes and in the Central Depression (see *Rech et al*. [2003] for in-depth descriptions of these samples and their isotopic ratios). Combining all these results, they defined a typical Andean weathering products' $^{87}Sr/^{86}Sr$ signature of 0.70749 ± 0.00046 [*Rech et al*., 2003]. *Vivallo and Henriquez* [1998] summarized $^{87}Sr/^{86}Sr$ for several major rock units in the Coastal Cordillera immediately south of our study area. They report that the widespread La Negra Formation and localized plutons have values limited to 0.703–0.704, whereas stratiform ore bodies are dominated by values of 0.704–0.706. These are whole rock rather than weathered products' Sr isotopic values, so that their comparison with the Andean average calculated by *Rech et al*. [2003] is not straightforward.

On the one hand, unconsolidated gravel sediments in dry stream beds below which we collected many of the calcium sulfate samples derive from Andean erosional source areas. On the other hand, for most of the cases of calcium sulfate sampled in association with eolian sediments, the sand was transported from the coastal region. Therefore, the parent rock for the stream bed gravel likely had a $^{87}Sr/^{86}Sr$ signature typical of the Andean average while eolian sand parents were more likely typical of the Coastal Cordillera.

Under the assumption that marine aerosols and Andean weathering products are the two main inputs of calcium sulfate salts to the Atacama Desert soils, an accumulation of salts that is a mixture of those inputs should develop an intermediate Sr isotopic ratio. The actual Sr isotopic value might be given by a linear mixing model between the two end-members:

$$x(^{87}Sr/^{86}Sr)_{marine} + (1-x)(^{87}Sr/^{86}Sr)_{Andes} = (^{87}Sr/^{86}Sr)_{salt} \quad (1)$$

where x is the contribution of marine aerosols to the Sr ratio of the salts, $(^{87}Sr/^{86}Sr)_{marine} = 0.70916$, and $(^{87}Sr/^{86}Sr)_{Andes} = 0.70749$ [*Rech et al*., 2003]. However, as we have seen in the previous paragraph, Coastal Cordillera weathering products also constitute an input of calcium sulfate salts to Atacama Desert soils. An alternative way to look at this problem, one that does not require the definition of an Andean rock Sr isotopic ratio average, will be presented in a later section.

Presented below are Sr isotopic composition and variations for a suite of samples of Holocene salts that accumulated across the Atacama Desert landscape over a wide area. Analysis of the $^{87}Sr/^{86}Sr$ data allows a comprehensive understanding of the effects of topography on the Sr isotopic ratio of Holocene surface salt accumulations at a regional scale. Knowledge of the dependence of Holocene Sr isotopic ratio on modern altitude is a foundation for interpretation of long time scale relationships of paleo-fog distribution to paleo-altitude across the continental surface.

3. Methods

3.1. Sampling of Landscape Salt Accumulations

In order to study the spatial variability of the $^{87}Sr/^{86}Sr$ signature of modern accumulations of salts precipitated on or reworked across the study area landscape, superficial unconsolidated materials were sampled at

38 sites (one sample per site) across two east-trending transects and at other specific sites (Figure 1). A published data set by *Rech et al*. [2003] is relevant for comparison, but their sampling strategy was notably different from the design of the current project, which limits the degree of intercomparison. Their 12 soil samples from south of the area sampled in this study were taken along two E–W transects and at other specific sites (Figure 1).

The four transects cover the Andean fore arc from the western Coastal Escarpment to the Andean foothills in the east, crossing the Coastal Cordillera and inner fore-arc basin. Altitudes range between ~200 and ~3000 masl, although most sample sites (45 out of 50) are located between ~200 and ~1900 masl.

The northernmost transect, Pisagua, is located at ~19.5°S (Figure 1). This ~40 km long transect samples the plain between the deeply incised Tana and Tiliviche canyons, from the junction of those two canyons on the west (at ~950 masl) to an altitude of ~1850 masl on the east. The ~70 km long Huara transect is located at ~20°S (Figure 1) and consists of samples of the Coastal Escarpment, Coastal Cordillera, fore-arc basin, and Andean foothills, with elevations varying between ~200 and ~2750 masl. The Tocopilla transect at ~22°S of *Rech et al.*'s [2003] extends ~65 km from the Pacific Ocean into high-grade nitrate deposits in the Central Depression, covering elevations between ~900 and ~1450 masl (Figure 1). The Antofagasta transect at ~24°S extends more than 200 km from the Coastal Escarpment to Cordillera Domeyko, with elevations between ~650 and ~3000 masl (Figure 1). In addition to these transects, 21 samples test other individual locations of interest, many of them at an elevation near 1100–1200 masl (Figure 1).

For collection of the superficial gypsum and anhydrite at the 38 new sites, the primary sample selection challenge was to distinguish between Holocene gypsum/anhydrite superficial materials and relict gypsic soils, and to avoid samples that might be contaminated by pre-Holocene gypsic soil. Given that relict gypsic soils are widespread on old landscape surfaces in the study area [*Jordan et al*., 2014], our strategy was to target the following landscape positions: (1) channels incised below the ancient landscape surfaces in which there were at least 10 cm thickness of postincision fluvial deposits overlying any relict soils, (2) wind-deflated pits that are eroded into the regional relict landscape surface, specifically seeking a part of a deflation pit with a layer of eolian sand overlying the predeflation soils or sediments and underlying the potential gypsum/anhydrite sample, and (3) the angle-of-repose slope of the Coastal Escarpment. In those small-scale landscape settings, we sought accumulations of gypsum or anhydrite. For the thin soft crust of the Coastal Escarpment or the tens of centimeter thick dust accumulations of some parts of the Coastal Cordillera and Central Depression, we collected samples from the most superficial 5 cm. For the incised fluvial channels and surfaces covered by eolian sand sheets, we turned over tens of cobbles and boulders to locate individual clasts under which gypsum crystals formed a soft crust. The samples were commonly collected with a spoon or a steel knife blade and placed in plastic sample bags. The occurrence category at each sample is reported in supporting information Table S1 (supporting information S1). Expertise in recognition of pre-Holocene gypsic soils improved over the 3 years of sampling, with the outcome that more of the 2011 samples are categorized as of low probability of being restricted to Holocene materials than for 2012 and 2013 sample years. Based on the sample and geomorphic context characteristics, we classified each sample by the probability that it consists of a recently (i.e., Holocene) deposited intermixture of salts and fine-grained siliciclastics (supporting information Table S1; supporting information S1).

The *Rech et al*. [2003] samples from the southern two transects were not collected specifically to capture the Holocene conditions. Those samples were obtained at depths of 20–30 cm below the top of the local soil, often from the upper part of a moderately cemented horizon. These samples represent longer time-averaged conditions. Along the *Rech et al*. [2003] southernmost profile, *Ewing et al*. [2008] sampled a vertical sequence inclusive of depths as shallow as 1 and 2.5 cm below the top of the local soil. Plausibly those shallowest horizons sample Holocene materials of a type similar to our third category of surface materials (Figure 2c). However, *Ewing et al.*'s [2006] criteria for selection of that site, i.e., that the landform position was morphologically higher than local stream beds and thus older than the modern depositional system, places it by our criteria in a category somewhat older than the materials on which we focus in this paper.

3.2 Fog Sampling

Three samples of fog water were collected at "fog-catcher" nets at Alto Patache (70.15°W, 20.83°S, see site TJ-103, TJ-104, and TJ-106 in Figure 1). The nets consist of plastic webbing mounted vertically on a wooden frame, through which the wind drives the fog. Water droplets drain off the web. Particulate contaminants,

apparently of deteriorated plastic net, were found in two of the samples that were collected from a PVC tube at the base of the net (TJ-104 and TJ-106). Fog sample TJ-103 was obtained on 3 September 2012, at 16.08–16.10 h (GMT-4).

3.3. Chemistry, Mineralogy, and Sr Isotopic Compositions

For each surface salt sample, the coarser-than-0.5 cm siliciclastic fraction was separated and the rest of the sample was physically homogenized and then soaked in water to dissolve the soluble salts. The ratio of water to sample necessary for full dissolution of the soluble fraction of the sample was determined by experimentation with different sample aliquots and water volumes. Those experiments led us to adopt a standard ratio of approximately 50 mg of the homogenized sample mixed with 35 ml of ultrapure water (resistivity of 18.2 MΩ cm), which was placed in an ultrasonic warm (~50°C) bath during 8 h, and finally centrifuged at 3000 rpm for 15 min.

The F^-, NO_3^-, Cl^-, and SO_4^{2-} concentrations of the resulting solution were measured using ion chromatography (Dionex ICS 2000, Cornell University), while the Ca^{2+}, Mg^{2+}, K^+, Na^+, Sr, and Si concentrations were determined using ICP-OES (Amteck SpectroBlue, Cornell University). Sr in some samples was measured by ICP mass spectrometry (Thermo-Finnigan Element2, Cornell University). In all cases, measurement uncertainty is better than 5%.

In the case of the fog samples, cation concentrations were obtained in the same manner, except for soluble Si. The concentration of Si was determined based on the absorbance of a silicomolybdate complex solution [*Mortlock and Froelich*, 1989], within 2% uncertainty.

Identification and quantification of mineral phases of selected bulk solid samples of surface salt accumulations were carried out using a Scintag Theta-Theta X-Ray Diffractometer (XRD, Cornell University). Phase quantification based on XRD analysis has many caveats [e. g., *Moore and Reynolds*, 1997; *Kahle et al*., 2002]. Thus, we present our phase quantification results as first-order estimates that make relative comparisons, rather than absolute determinations, possible.

Finally, all solutions (including fog sample TJ-103) were passed through cation-exchange columns, using *Eichrom Sr* as the ion-exchange resin, and using the methodology proposed by *Horwitz et al*. [1992]. For most samples, $^{87}Sr/^{86}Sr$ was measured with thermal ionization mass spectrometry (VG Sector 54, Cornell University). NBS-987 Sr standards run in association with samples averaged 0.71024 ± 0.00003 (2σ, n = 32). For samples NC13-138, NC13-145, NC13-152, NC13-153, and NC13-156, and for fog sample TJ-103, $^{87}Sr/^{86}Sr$ was measured with a Neptune Multicollector ICP-MS (Rutgers University). In this case, NBS-987 Sr standards run in association with samples averaged 0.710282 ± 0.000012 (2σ, n = 18). In both cases, the water:sample ratio used (200 mg of sample and 10 mL water volume) during the soluble salt extraction process was different from the one discussed above for the case of the determination of the chemistry of the samples. Apart from this difference, the process was the same. Sr isotopic measurements were performed for a subset of eight samples using both extraction water:sample ratios, and in all cases the differences in $^{87}Sr/^{86}Sr$ lay in the fifth decimal, or within 2σ of each other. Thus, even though dissolution of gypsum in the 20 ml:200 mg experiments may have been incomplete, the results demonstrate that there was not an impact on $^{87}Sr/^{86}Sr$ which would be a concern if various calcium sulfate components bore differing $^{87}Sr/^{86}Sr$.

4. Results and Discussion

4.1. Chemistry of the Soluble Fraction of the Samples and Sr Isotopic Compositions

The chemical composition of the soluble fraction of the landscape surface samples is dominated by Ca^{2+} and SO_4^{2-} (averages of 1.56 and 1.37 mmol/g of total sample, respectively, supporting information Table S1). Na^+ and Cl^- occur in intermediate quantities (0.26 and 0.22 mmol/g, respectively, supporting information Table S1), while NO_3^-, K^+, and Mg^{2+} are found in small quantities (0.023, 0.019, and 0.020 mmol/g, respectively). Sr and F^- occur in trace amounts (0.002 and 0.003 mmol/g, respectively, supporting information Table S1). Finally, the average content of soluble Si is 0.068 mmol/g (supporting information Table S1).

There is a general equimolar trend in Ca^{2+} versus SO_4^{2-} (Figure 3a), and a less clear one for Na^+ versus Cl^- (Figure 3b). Samples in subgroups of high, low, and intermediate confidence that they represent Holocene

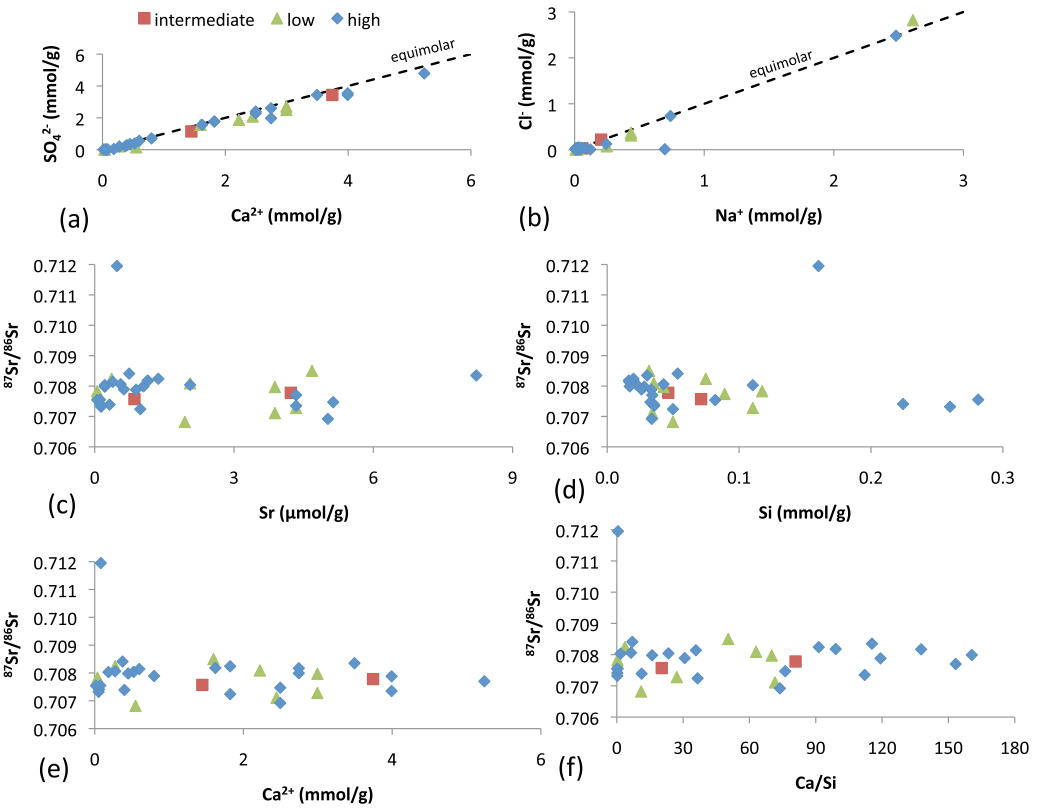

Figure 3. Chemistry and Sr isotopic ratio of the soluble fraction of modern accumulations of salt/siliciclastic samples. (a) Ca^{2+} versus SO_4^{2-}, (b) Na^+ versus Cl^-, (c) Sr versus $^{87}Sr/^{86}Sr$, (d) Si versus $^{87}Sr/^{86}Sr$, (e) Ca^{2+} versus $^{87}Sr/^{86}Sr$, and (f) Ca/Si versus $^{87}Sr/^{86}Sr$. Chemistry is expressed per gram of total solid sample. Color coded according to the confidence of recent deposition: blue for high, red for intermediate, and green for low confidence (see text for discussion).

deposition (supporting information Table S1) all yield equal molar ratios. The chemistry and molar trends are consistent with calcium sulfates being the main soluble mineralogical phases.

Sr isotope ratios range between 0.70682 and 0.70850, with one outlier at 0.71195 (NC11-33, supporting information Table S1, Figure 3). There is no apparent correlation between $^{87}Sr/^{86}Sr$ and the concentrations of soluble Sr (Figure 3c), Si (Figure 3d), and Ca (Figure 3e). No specific trends are observed for any subgroup of samples based on the confidence of recent deposition (Figures 3c, 3d, and 3e). The only outlier, sample NC11-33, has one of the lowest Ca/Si ratios (Figure 3f), which suggests that a component of silicate-derived Sr may be important.

4.2. Mineralogy

Four samples from the Huara transect and one from the Pisagua transect were selected for XRD analysis of mineralogy (Table 1; see Figure 4 for site locations).

For the Huara transect, bulk mineralogy is dominated by gypsum for the two sites below 800 masl, with 70% gypsum by mass. Samples collected further from the coast and above 1200 masl (NC11-8 and NC11-12) show a dominance of anhydrite over gypsum. The sample collected at ~1210 masl is mostly composed of anhydrite, while the sample collected at ~2770 masl has a dominance of quartz (80%). The Pisagua transect sample NC12-74, at ~1180 masl, contains ~30% gypsum, with the rest of the mass composed of silicates (quartz and plagioclase).

The results show that gypsum dominates at lower elevations while anhydrite is favored at higher altitudes. Furthermore, the highest salt fractions are found at low elevations. This elevation dependence of the salt composition and its fraction of the total incipient soil mass suggest a strong marine aerosol control. We infer that these trends occur because (a) gypsum is the favored calcium sulfate phase during wet and dry

Table 1. Mineralogy of Modern Accumulation of Salt Samples[a]

Sample	Location	Distance From Coast (km)	Altitude (±30 masl)	Phases	Comments[b]
NC11-4	19°52′46.80″S 70°07′35.04″W	0.9	260	Gyp: 70% Cal: 20% Qz: 10%	Huara transect. Salt-cemented, indurated surficial crust. Coastal escarpment. High confidence.[c]
NC11-6	19°56′39.08″S 70°03′06.63″W	10.3	750	Gyp: 70% Qz: 30%	Huara transect. Light tan powdery material below gravel. Coastal Cordillera. Low confidence[c].
NC11-8	19°57′47.39″S 69°37′30.07″W	54.4	1210	Anh: 100%	Huara transect. White powdery material below gravel. Central Depression. High confidence.[c]
NC11-12	19°45′27.01″S 69°15′56.73″W	93.6	2770	Qz: 80% Anh: 20%	Huara transect. White powdery material below gravel. Central Depression. High confidence.[c]
NC12-74	19°29′01.33″S 69°52′46.51″W	35.5	1180	Qz: 40% Plg: 30% Gyp: 30%	Pisagua transect. White powdery material below gravel. Central Depression. High confidence.[c]

[a]XRD analysis of selected modern accumulation of salts samples.
[b]See text for detailed sample description and for discussion of phase quantification uncertainty.
[c]Confidence that sample represents recently deposited (Holocene) materials. See text for discussion.

marine aerosol precipitation and (b) an enhanced availability of marine aerosols at low elevation produces a high salt-to-siliciclastics ratio.

No halite phase was identified among the major minerals by XRD. Nonetheless, Na and Cl could be present as subordinate halite, or as part of other mineral phases. Na and Cl may be also present as adsorbed ions on the exchange complexes of silicate clays.

4.3. $^{87}Sr/^{86}Sr$ Variations Inland From the Coast

4.3.1. $^{87}Sr/^{86}Sr$ of Fog Water at the Coastal Escarpment

The $^{87}Sr/^{86}Sr$ value obtained (sample TJ12-103, 0.70875 ± 0.00001, see supporting information Table S1) is lower than seawater $^{87}Sr/^{86}Sr$ (0.70916) [*Farrell et al*., 1995]. However, the ratio is higher than for any other material sampled by *Rech et al*. [2003] or for this study (except the outlier, sample NC11-33).

4.3.2. Huara Transect

The Huara transect crosses the Coastal Escarpment, Coastal Cordillera, and Central Depression in a zone lacking cross-fore-arc fluvial drainage, where the escarpment relief is approximately 750 m. This transect consists of 12 sampling sites (Figure 4b), nine of which were classified as unambiguously Holocene, two as likely Holocene, and one as sufficiently ambiguous that we omit it from further consideration (supporting information Table S1).

Considering only samples that are assumed modern with intermediate to high certainty (yellow and blue samples, Figure 4b), the highest $^{87}Sr/^{86}Sr$ values along the Huara transect are located inside the observational fog zone, peaking at the site ~1 km from the coast on the Coastal Escarpment (NC13-152, 399 masl), where the mixing model indicates ~32% marine contribution (Andean end-member: 0.70749). $^{87}Sr/^{86}Sr$ values along the Coastal Escarpment decrease toward the shoreline, reaching values indistinguishable from the Andean average at ~200 masl. To the east, the $^{87}Sr/^{86}Sr$ of modern salts decrease until reaching values similar to or lower than the Andean average at distances of ~40 km or more from the coast.

4.3.3. Pisagua Transect

The Pisagua transect was designed to explore the fog-related $^{87}Sr/^{86}Sr$ signal where there is a breach in the Coastal Escarpment and Coastal Cordillera through which fog penetrates farther to the east than is the case over most of the fore arc. The Central Depression at this latitude is incised by two fluvial valleys (Quebradas Tana and Tiliviche, Figure 4a) that parallel to each other before merging, at the eastern limit of the Coastal Cordillera, into a single valley. The single valley drains ~15 km distance to the Pacific Ocean and is deeply incised (~700 m) through the Coastal Cordillera. Along the Tana valley, the vertical incision through the Central Depression decreases to ~100 m at intermediate positions of the Central Depression, and increases

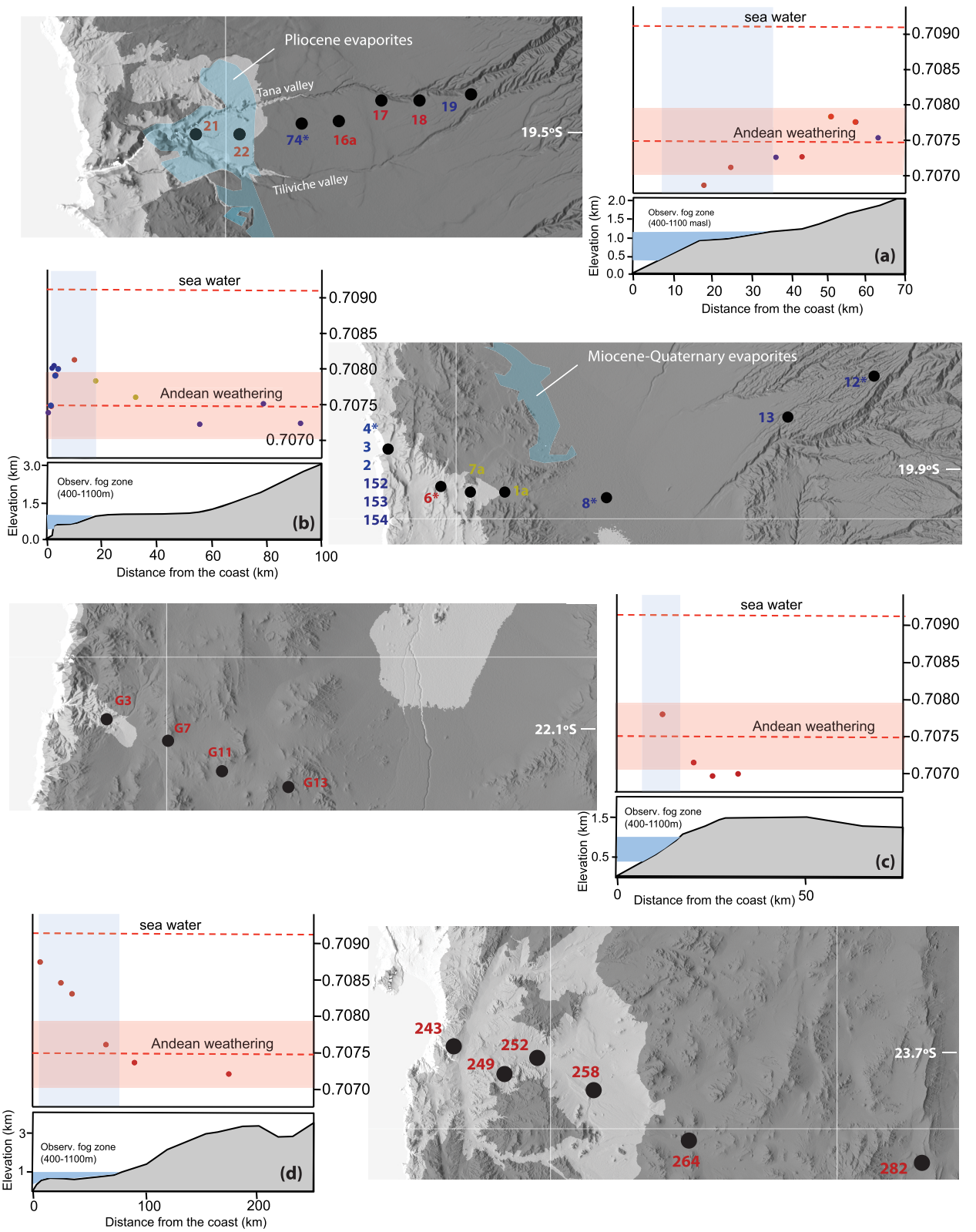

Figure 4. Sampled locations along the ~E–W transects and $^{87}Sr/^{86}Sr$ results plotted against distance to the coast for (a) Pisagua transect, (b) Huara transect, (c) Tocopilla transect, and (d) Antofagasta transect. Shown in light blue is the area with altitudes between 400 and 1100 masl (coastal fog zone). Samples for which XRD analysis was performed are asterisked (*). Samples with blue (yellow; red) font in the map and blue (yellow, red) dots in the graphs have a high (intermediate; low) certainty of having been formed in the Holocene. Seawater $^{87}Sr/^{86}Sr$ taken from *Farrell et al.* [1995] and Andean weathering $^{87}Sr/^{86}Sr$ average from *Rech et al.* [2003], including uncertainty (pink box).

again to ~300 m at the easternmost sites. The inter-canyon plain is less incised along the Tiliviche valley, reaching ~40 m at intermediate transect sites, and ~170 m at the easternmost sites. All seven sites along this transect lie on the plain between the two valleys (Figure 4a).

Few of the samples in this transect meet the criteria to be assigned a high probability that they include only Holocene-age materials. In retrospect, this is a logical consequence of the two incised canyons bounding the plain; those canyons divert surface runoff from the adjacent Andean foothill ranges away from the inter-canyon plain. The result is uncharacteristically little fluvial erosion of the fore-arc basin, and thus there are very few diagnostic late Pleistocene or Holocene fluvial deposits with which to distinguish Holocene gypsum and anhydrite from pre-Holocene soil. Both of the samples that are categorized as having a high likelihood of a Holocene age (NC11-74 and NC11-19) are located at elevations that are today above the observational fog zone (1183 and 1870 masl, respectively). Their Sr ratios (0.70724 and 0. 70755, respectively) are consistent with little to no marine aerosol contribution.

The samples located at the western tip of the Tana/Tiliviche interfluve (~18 and ~25 km from the coast, westernmost two sites; NC11-21 and NC11-22) were sampled from the best available superficial materials, in eolian deflation pits. However, they are in proximity (1–3 cm) to bedded Pliocene evaporites, a salt pan that was active at 3.5 Ma [*Kirk-Lawlor et al*., 2013] in locations frequently wet by fog. Therefore, we judge that there is a high likelihood for contamination. Because those samples show the lowest $^{87}Sr/^{86}Sr$ values of the transect, the $^{87}Sr/^{86}Sr$ values increase with distance inland, an unexpected trend. This deviation is interpreted to result from the remobilization of salar dust toward sampling sites NC11-21 and NC11-22, thereby acquiring an isotopically light gypsum component [*Rech et al*., 2003], which would obscure a fog signal even if marine aerosols do indeed contribute to modern salts in that area.

4.3.4. Antofagasta and Tocopilla Transects

These two transects are located between 22°S and 24°S and were previously reported by *Rech et al*. [2003]. Unlike the transects reported above, *Rech et al*. [2003] did not attempt to sample only Holocene materials. *Amundson et al*. [2012] provided evidence that along the Antofagasta transect the oldest superficial materials that one would encounter are younger than 2 Ma, hence this set of samples should be considered to represent the Quaternary conditions but not strictly the Holocene. With that limitation, these $^{87}Sr/^{86}Sr$ values were the original justification for hypothesizing an altitudinal dependence.

The Antofagasta transect has soil gypsum/anhydrite $^{87}Sr/^{86}Sr$ values that systematically decrease with distance from the Pacific Ocean (Figure 4d). Using the two end-member linear mixing model (1), the westernmost sample shows a marine component of ~80% (Andean end-member: 0.70749), while samples more than 50 km from the coast become indistinguishable from the Andean average, as defined by *Rech et al*. [2003]. *Ewing et al*. [2008] sampled a vertical profile of an ancient soil located ~30 km to the southwest of the Antofagasta transect at 24.10°S, 70.02°W, at an altitude of 1020 masl. This ancient soil is 2.3 m thick and is younger than 2.1 Ma [*Ewing et al*., 2008]. The $^{87}Sr/^{86}Sr$ values decrease from 0.70743 at 1 cm depth to 0.70709 at 134 cm depth [*Ewing et al*., 2008]. AT258 and AT264 are Antofagasta transect samples located at 845 and 1305 masl, respectively (supporting information Table S1). They were sampled at depths of 20–30 cm and have $^{87}Sr/^{86}Sr$ values of 0.70761 and 0.70736, respectively (supporting information Table S1). At similar depths below the ancient soil top, the *Ewing et al*. [2008] profile has values of 0.70740 and 0.70733. The shallowest sample at this profile, which is the one that is arguably more likely to have the greatest Holocene contribution, has a $^{87}Sr/^{86}Sr$ value of 0.70743, very close to the Andean average by *Rech et al*. [2003].

The Tocopilla transect (Figure 4c) shows that the sample with highest $^{87}Sr/^{86}Sr$ is the one within the observational fog zone, at ~10 km from the coast. The rest of the samples were all collected outside the observational fog zone and have $^{87}Sr/^{86}Sr$ values below the Andean average (Figure 4c).

4.4. $^{87}Sr/^{86}Sr$ Altimetry

A graph of the altitude of salt accumulation and the Sr isotope signature that is inclusive of all samples ($n = 50$; Figure 5a) displays a general trend of high ratios at low elevation and a $^{87}Sr/^{86}Sr$ decline as elevation increases. However, a meaningful comparison of this result to the known fog climatology requires that we narrow the data to salts formed during the time of stable climate. Therefore, the data set was filtered to exclude the sites previously categorized as low likelihood that they are Holocene, which leaves 28 data points (Figure 5b; supporting information Table S1). A sample-by-sample analysis of these criteria can be found in supporting information Figures S1–S15.

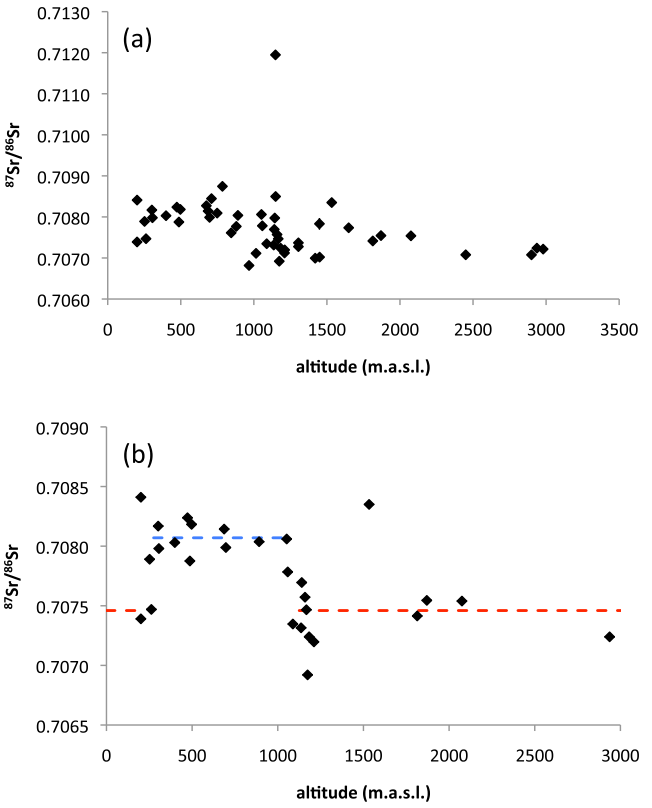

Figure 5. (a) Modern accumulations of salts' $^{87}Sr/^{86}Sr$ and altitude of formation for the whole data set. (b) Subset of samples with high and intermediate certainty of recent deposition (see text for discussion). The red dashed line represents the bootstrap value for the time-averaged outside-of-the-fog isotopic ratio, while the blue dashed line corresponds to the inside-of-the-fog equivalent.

In the complete data set, $^{87}Sr/^{86}Sr$ varies between 0.70682 and 0.70875, with an outlier at 0.71195 (~1150 masl). The highest ratios are found at low altitudes (89% of all ratios higher than 0.7079 are located lower than 1150 masl). Also, there is an altitudinal band with high variability around 1150 masl.

The outlier NC11-33 has a high likelihood of being Holocene (supporting information Table S1). It also has one of the lowest Ca/Si ratio of the data set, which suggests that an important component of its Sr is probably derived from silicate Ca. This could occur because of inclusion of adsorbed cations that were located in the exchange complexes of micas, which can be easily incorporated into the aqueous solutions that result from our separation procedure. This outlier is not considered further.

In the age-filtered data set, we distinguish three altitudinal bands (Figure 5b). The first band contains samples located between ~300 and ~1050 masl where $^{87}Sr/^{86}Sr$ is higher than or equal to 0.70788 and there is relatively little variability. A second altitudinal band is identified below 300 masl, where two sites show low $^{87}Sr/^{86}Sr$ values, and one shows a high $^{87}Sr/^{86}Sr$ value. In the third band, for altitudes exceeding 1150 masl, six out of seven samples show values that are below the lowest ratio in the 300–1050 masl altitudinal band (the exception is NC11-49, 1533 masl). Samples located near 1100 masl display a high degree of variability of the $^{87}Sr/^{86}Sr$ values yet that variability is less than in the unfiltered data set.

We argue that the $^{87}Sr/^{86}Sr$ versus altitude distribution for Holocene salt shows the contribution of the average Holocene (since ~10,000 years ago) marine aerosol system to the superficial deposits. In this sense, the *averaged-in-time fog zone* would correspond to the altitudinal band with highest $^{87}Sr/^{86}Sr$ ratios, ~300 and ~1050 masl. Whereas visual inspection shows ~1100 masl to correspond to the averaged-in-time fog zone upper limit, investigation of this critical boundary region is warranted. An important characteristic of the data set is that some altitudes have been sampled more densely than others. Therefore, to explore for detailed trends in the data requires the use of an estimator of mean deviation that normalizes for the number of samples (N) at each elevation. Division of the altitude domain into 100 m bins and calculation of the unbiased standard error of the mean (s, where $s = \sigma$/&cenveo_unknown_entity_Symbol_F0D6;N and σ is the unbiased standard deviation) for each bin determines that the 1000–1100 masl bin has the highest s value (0.00021), compared to 0.00011 for the next highest s value corresponding to the 1100–1200 masl bin. Changing the bin width to 50 masl reveals that the 1050–1100 masl bin has the highest unbiased standard deviation, s.

An alternative approach is to compare two data samples using the Kolmogorov-Smirnov nonparametric test, which quantifies the difference between the two empirical distribution functions of two samples. In this case, these two samples correspond to the samples defined below and above a given altitude threshold. By conducting this test for several altitude thresholds, we can decide on the most probable time-

averaged fog top as the one with the greatest difference between sample sets. For altitudes every 25 m between 1050 and 1250 masl, the two sample sets are most different for an altitude threshold of 1075 masl.

These results identify the upper time-averaged fog top at 1075 masl. Significantly, the top boundary for the high $^{87}Sr/^{86}Sr$ domain falls within DEM error of the previously defined observational top-of-the-fog altitude at 1100 masl [*Cereceda et al*., 2002; *Farías et al*., 2005a].

With respect to the lower altitudinal boundary for the fog-influenced domain, visual inspection suggests a high variability between 200 and 250 masl. A statistical analysis similar to that done for the top-of-the-fog zone is not possible due to far fewer data points. Further sampling and measurements may improve the definition of a time-averaged lower marine aerosol boundary.

Distance from the coast and local, short-scale topographic variability may also explain in part the distribution of $^{87}Sr/^{86}Sr$ of Holocene salt accumulations. Studies of the spatial distribution of modern fog reveal significantly higher frequency of fog events in certain topographic corridors that transect the Coastal Cordillera [*Farías et al*., 2005a]. We reason that those effects of complex topographic patterns that block or enhance air mass flow may in part explain variability within each domain (inside and outside the Holocene fog zone). Given the clear altitudinal control of the observational fog top, the first-order bimodal nature of the $^{87}Sr/^{86}Sr$ distribution is best explained by altitude.

In summary, we interpret the domain between ~225 and 1075 masl to represent the land area under marine fog influence. Since salts sampled during our studies are younger than 10,000 years, these domain boundaries are interpreted as averaged over that time period.

4.5. Bootstrap Analysis

Although *Rech et al*. [2003] offered one approach to quantifying the $^{87}Sr/^{86}Sr$ of an Andean end-member for the mixed sources of salts in Atacama modern soils (section 2.5), the robustness of that number depends upon whether the included samples are fully representative of all the nonmarine processes affecting the Sr isotopic ratio. We can avoid making such assumptions by following another approach based on the statistical properties of the new data sets (supporting information Table S1). In this new approach, we conceptualize a background Sr isotopic ratio, upon which deposition of salts from marine aerosols causes modification of this ratio. That background $^{87}Sr/^{86}Sr$ value would be the Andean average.

Commonly, geochemical variables are not normally distributed (and not lognormally distributed, for that matter), since many processes are at work to define elemental concentration or isotopic ratios in a given rock. Taking advantage of computer-intensive statistical methods such as *bootstrapping* [*Efron*, 1979], it is not necessary to assume a prior mathematical form for a given distribution at all. Instead, we can use our existing set of samples as an approximation of the underlying population. Specifically, given a data set of size *n*, take samples with replacement of size *n* from that data set to approximate samples of size *n* from the underlying population. In order to estimate the background modern (i.e., filtered data set) nonmarine Sr ratio and its standard error:

i. randomly sample one isotope ratio from the complete n = 12 subdata set (number of outside-of-the-fog soil samples), then repeat this 11 times, and finally compute x (mean) of these 12 randomly sampled isotope ratios,
ii. repeat step i a sufficient number of times *B* to come up with "bootstrap" estimates x_1, x_2, . . ., x_B, and
iii. use the standard deviation of the *B* estimates in step ii to estimate the standard error.

The estimate of mean and standard error of the mean converge quickly to 0.70746 and 0.00010, respectively, with high values of *B* (Figure 5). This is then the background Sr ratio of modern accumulations of salts in the Atacama Desert, unaffected by marine fog. It coincides within error to 0.70749 ± 0.00046, the Andean average as defined by *Rech et al*. [2003].

Doing this same analysis with the inside-of-the-fog data set (n = 9), we obtain a value of 0.70807 ± 0.00004 (Figure 5). Thus, those two data sets belong to different populations. This reinforces our interpretation that the participation of marine fog in formation of superficial calcium sulfate minerals in the Atacama Desert has a clear signature in the resultant $^{87}Sr/^{86}Sr$. This reinforces previous studies that reached the same conclusion [*Rech et al*., 2003]. Note that neither the samples that fall within the high-variability altitudinal band

centered on 1075 masl (time-averaged fog top) nor samples collected between 200 and 275 masl were considered for the bootstrapping.

5. Implications for $^{87}Sr/^{86}Sr$ Paleoaltimetry

These results show that $^{87}Sr/^{86}Sr$ of modern accumulations of salts in the Atacama Desert, northern Chile, provide a proxy for their altitude of formation. The distribution with altitude of the Sr isotopic ratios is bimodal with two threshold elevations (~225 and 1075 masl). If a comparable relationship existed for salts that formed soils during the late Miocene through Pleistocene, then the $^{87}Sr/^{86}Sr$ value of pre-Holocene calcium sulfate may provide a measure of paleoaltitude that would be useful for quantifying tectonically driven surface uplift or subsidence of the Andean fore arc. As shown by *Rech et al*. [2006], *Ewing et al*. [2008], and *Jordan et al*. [2014], post-10 Ma buried Gypsisols and exposed relict gypsic soils are widespread and suitable for this paleoaltitude proxy.

The fundamental strategy of this potential paleoaltimeter is that the band of elevations above sea level in which marine fog supplies aerosols to the continental surface provides a reference altitude in a sea level reference frame. To consider the premises necessary for use of this paleoaltimeter, we consider the conditions extant during the Holocene and the likelihood of their stability into the deep geological past. The stability through time of the fog system along the western edge of South America is closely related to the stability of the low-altitude atmospheric temperature inversion in the area. The temperature inversion depends on the combination of regional atmospheric subsidence, cold offshore surface waters and to a lesser extent, the existence of the Andean highlands (section 2.1). The stability of regional atmospheric subsidence in the area is accepted as a result of an almost unchanged latitudinal position of the continent since 150 Ma [e.g., *Beck et al*., 2000]. The temperature of near-coastal waters has been like that of the modern Humboldt system at least since the middle Miocene [*Amiot et al*., 2008]. Finally, more than half of the height of the modern western Andes Cordillera was achieved during the lower middle Miocene [*Gregory-Wodzicki*, 2000; *Victor et al*., 2004; *Farías et al*., 2005b]. Thus, it is to be expected that a persistent offshore low-altitude atmospheric inversion layer existed since at least mid-Miocene times, although its altitude need not have been constant.

The ability of geological materials like gypsum and anhydrite to capture an environmental Sr ratio requires that there existed a climate prone to evaporation of fog and crystallization of calcium sulfate. *Sillitoe and McKee* [1996], *Dunai et al*. [2005], *Rech et al*. [2006], and *Jordan et al*. [2014] presented the evidence that hyperarid conditions have been typical in the northern Chile fore arc for more than 10 million years, although interrupted multiple times for intervals of arid conditions that persisted several hundred thousand to 1 million years [*Jordan et al*., 2014]. Therefore, both an analogous paleo-fog system and ancient superficial calcium sulfate deposits may have existed in Atacama Desert.

However, even if analogous relations of altitude to Sr ratio existed during the late Miocene and Pliocene, it is unlikely that the altitudes of the thresholds and the $^{87}Sr/^{86}Sr$ values were equal to those in the recent past. Several factors of the atmosphere-ocean-land system, both global and local, likely have varied. First, the marine aerosol $^{87}Sr/^{86}Sr$ end-member is anchored to seawater $^{87}Sr/^{86}Sr$, which has changed with time. The secular trend of seawater $^{87}Sr/^{86}Sr$ is well known for the Neogene, rising from 0.70891 to 0.70917 since 10 Ma [*Hodell et al*., 1991; *Farrell et al*., 1995]. Second, climate change affects the atmospheric temperature inversion layer and with it the height of the top of the cloud deck above the sea surface [*Wang et al*., 2004]. Third, global sea level change as well as regional tectonics will both have changed the position of the intersection of sea level with the fore-arc morphology in a rock reference frame. Even if the "elevation above sea level" of the stratocumulus clouds were to have been constant in a sea level reference frame, global sea level change would alter the intersection of both sea level as well as the stratocumuli clouds with the continental surface in a rock-based reference frame. If the objective is to deduce tectonic uplift or subsidence, then the global sea level change with a magnitude of approximately 175 m during the past 10 million years [*Miller et al*., 2005] is an interfering signal.

The results presented here lead to the definition of criteria to decide whether a given paleosol was formed inside or outside the paleo-fog zone that existed while the soil formed. One way to do this is to use the distribution of the outside-of-the-fog calcium sulfate data set and, under the bootstrap approximation that it coincides with the underlying population, define a likelihood that a given paleosol (with a given $^{87}Sr/^{86}Sr$ ratio) did not form outside the paleo-fog zone. For a given paleosol with a $^{87}Sr/^{86}Sr$ value of x, and a given

outside-of-the-fog sample size *n*, the likelihood of this paleosol having formed inside-of-the-fog zone is 100 × (p/n), where *p* is the number of outside-of-the-fog soil samples with $^{87}Sr/^{86}Sr$ lower than x.

6. Conclusions

We have developed a new bimodal modern altitude proxy for continental surfaces in the Atacama Desert based on $^{87}Sr/^{86}Sr$ of Holocene superficial salt accumulations. The altitude-dependent phenomenon that underlies this proxy is the first-order topographic control on the spatial extent of marine fog events that advect aerosols inland from the southeast Pacific. As was shown in previous studies [e.g., *Rech et al*., 2003], evaporation of the water deposited on the land surface from the fog precipitates calcium sulfates on the landscape and is one of the main contributors of gypsum and anhydrite to calcium sulfate dust and crusts in the Atacama Desert. On average during the last ~10,000 years, the isotopic signature of marine aerosol Sr precipitated as calcium sulfates between ~225 and 1075 masl is distinctly higher than $^{87}Sr/^{86}Sr$ of salts sampled outside this altitudinal domain. This Sr isotopic distinction provides a proxy that defines two altitudinal domains. This proxy has been shown to be effective along a ~200 km latitudinal band (19.5°S–21.5°S).

Given a set of paleosols of known age, it may be possible to use this novel method as a paleoaltitude proxy. In order to do so, the polygenetic origin of the surficial salt accumulations as well as pedogenesis along vertical profiles of paleosols and/or relict soils, among other considerations, requires further scrutiny. Corrections that must be applied in order to isolate signals related to progressive topographic change include temporal variations in seawater $^{87}Sr/^{86}Sr$, global sea level changes, and changes in the structure of the atmospheric inversion layer. This is a promising method with which to constrain the tectonic uplift history of the Nazca-South America fore arc in northern Chile.

Acknowledgments

Financial support for this work was provided by National Science Foundation award EAR-1049978 to TEJ and JPM. The authors are grateful for the logistic services of Antonio Díaz during fieldwork. Field discussions with Arturo Jensen and Felipe Andrés Lobos Roco and laboratory discussions with and contributions by Naomi Kirk-Lawlor, Natalie Mahowald, Paola Vannucchi, William White, Linda Godfrey, Gregg McElwee, Kyle Torstle, and Jason Rech contributed to the development of this study. An anonymous reviewer and Greg Michalski are thanked for their very constructive reviews. Supporting data are included as an extra table in .xls format; any additional data may be obtained from NJC (njc58@cornell.edu).

References

Amiot, R., U. B. Gohlich, C. Lécuyer, C. de Muizon, H. Cappetta, F. Fourel, M. Héran, and F. Martineau (2008), Oxygen isotope compositions of phosphate from Middle Miocene-Early Pliocene marine vertebrates of Peru, *Palaeogeogr. Palaeoclimatol. Palaeoecol.*, *264*, 85–92.

Amundson, R., W. Dietrich, D. Bellugi, S. Ewing, K. Nishiizumi, G. Chong, J. Owen, R. Finkel, A. Heimsath, and B. Stewart (2012), Geomorphologic evidence for the late Pliocene onset of hyperaridity in the Atacama Desert, *Geol. Soc. Am. Bull.*, *124*, 1048–1070.

Azúa-Bustos, A., C. González-Silva, R. A. Mancilla, L. Salas, B. Gómez-Silva, C. P. McKay, and R. Vicuña (2011), Hypolithic cyanobacteria supported mainly by fog in the coastal range of the Atacama Desert, *Microbial Ecol.*, *61*(3), 568–581, doi:10.1007/s00248-010-9784-5.

Beck, M., R. Bermester, J. Cembrano, R. Drake, A. García, F. Hervé, and F. Munizaga (2000), Paleomagnetism of the North Patagonian Batolith, southern Chile. An exercise in shape analysis, *Tectonophysics*, *326*(1–2), 185–202.

Bourgois, J. (2010), A comment on "Non-steady long-term uplift rates and Pleistocene marine terrace development along the Andean margin of Chile (31°S) inferred from ^{10}Be dating" by M. Saillard, S. R. Hall, L. Audin, D. L. Farber, G. Hérail, J. Martinod, V. Regard, R. C. Finkel, F. Bondoux, *Earth Planet. Sci. Lett.*, *296*(3), 502–505.

Cereceda, P., and R. S. Schemenauer (1998), Fogwater collection at El Tofo, Chile and other coastal sites in South America and Arabia, in *Proceedings of the First International Conference on Fog and Fog Collection*, edited by R. S. Schemenauer and H. Bridgman, pp. 409–411.

Cereceda, P., R. S. Schemenauer, and F. Velásquez (1997), Variación temporal de la niebla en El Tofo-Chungungo, Región de Coquimbo, Chile, *Rev. Geogr. Norte Grande*, *24*, 191–193.

Cereceda, P., P. Osses, H. Larrain, M. Farías, M. Lagos, R. Pinto, and R. S. Schemenauer (2002), Advective, orographic and radiation fog in the Tarapacá region, Chile, *Atmos. Res.*, *64*, 261–271.

Comte, D., and M. Pardo (1991), Reappraisal of great historical earthquakes in the northern Chile and southern Peru seismic gaps, *Nat. Hazards*, *4*, 23–44.

Dunai, T. J., G. A. González López, and J. Juez-Larré (2005), Oligocene-Miocene age of aridity in the Atacama Desert revealed by exposure dating of erosion-sensitive landforms, *Geology*, *33*(4), 321–324.

Efron, B. (1979), Bootstrap methods: Another Look at the Jackknife, *Ann. Stat.*, *7*(1), 1–26.

Espejo, R. (2001), Climatological and microbiological characteristics of the camanchaca phenomenon at Cerro Moreno, Antofagasta, Chile, in *Proceedings of the Second International Conference on Fog and Fog Collection*, edited by R. S. Schemenauer and H. Puxbaum, pp. 463–466.

Ewing, S. A., B. Sutter, J. Owen, K. Nishiizumi, W. Sharp, S. S. Cliff, K. Perry, W. Dietrich, C. P. McKay, and R. Amundson (2006), A threshold in soil formation at Earth's arid-hyperarid transition, *Geochim. Cosmochim. Acta*, *70*, 5293–5322.

Ewing, S. A., W. Yang, D. J. DePaolo, G. Michalski, C. Kendall, B. W. Stewart, M. Thiemens, and R. Amundson (2008), Non-biological fractionation of stable Ca isotopes in soils of the Atacama Desert, Chile, *Geochim. Cosmochim. Acta*, *72*, 1096–1100.

Farías, M., P. Cereceda, P. Osses, and R. Núnez (2005a), Spatial and temporal behavior of the stratocumulus cloud, fog producer in the coast of the Atacama desert (21° south lat., 70° west long.), during one month of winter and another of summer, *Invest. Geogr. Boletín Inst. Geogr., UNAM*, *56*, 43–61.

Farías, M., R. Charrier, D. Comte, J. Martinod, and G. Hérail (2005b), Late Cenozoic deformation and uplift of the western flank of the Altiplano: Evidence from the depositional, tectonic, and geomorphologic evolution and shallow seismic activity (northern Chile at 19°30′S), *Tectonics*, *24*, TC4001, doi:10.1029/2004TC001667.

Farías, M., R. Charrier, S. Carretier, J. Martinod, A. Fock, D. Campbell, J. Cáceres, and D. Comte (2008), Late Miocene high and rapid surface uplift and its erosional response in the Andes of central Chile (33°–35°S), *Tectonics*, *27*, TC1005, doi:10.1029/2006TC002046.

Farrell, J. W., S. C. Clemens, and L. P. Gromet (1995), Improved chronostratigraphic reference curve of late Neogene seawater $^{87}Sr/^{86}Sr$, *Geology*, *23*, 403–406.

Ferranti, L., C. Monaco, F. Antonioli, L. Maschio, S. Kershaw, and V. Verrubbi (2007), The contribution of regional uplift and coseismic slip to the vertical crustal motion in the Messina Straits, southern Italy: Evidence from raised Late Holocene shorelines, *J. Geophys. Res.*, *112*, B06401, doi:10.1029/2006JB004473.

Garzione, C. N., G. D. Hoke, J. C. Libarkin, S. Withers, B. J. MacFadden, J. M. Eiler, P. Gosh, and A. Mulch (2008), Rise of the Andes, *Science*, *320*, 1304–1307.

Gayó, E. M., C. Latorre, T. E. Jordan, P. L. Nester, S. A. Estay, K. F. Ojeda, and C. M. Santoro (2012), Late Quaternary hydrological and ecological changes in the hyperarid core of the northern Atacama Desert (∼21°S), *Earth Sci. Rev.*, *113*, 120–140.

Gregory-Wodzicki, K. M. (2000), Uplift history of the Central and Northern Andes: A review, *Geol. Soc. Am. Bull.*, *112*, 1091–1105.

Herrera, C., and E. Custodio (2014), Origin of waters from small springs located at the northern coast of Chile, in the vicinity of Antofagasta, *Andean Geol.*, *41*, 314–341.

Hodell, D. A., P. A. Mueller, and J. R. Garrido (1991), Variations in the strontium isotopic composition of seawater during the Neogene, *Geology*, *19*, 24–27.

Hoke, G. D., B. L. Isacks, T. E. Jordan, N. Blanco, A. J. Tomlinson, and J. Ramezani (2007), Geomorphic evidence for post-10 Ma uplift of the western flank of the central Andes, 18°30′–22°S, *Tectonics*, *26*, TC5021, doi:10.1029/2006TC002082.

Horwitz, E. P., R. Chiarizia, and M. L. Dietz (1992), A novel strontium-selective extraction chromatographic resin, *Solvent Extraction Ion Exch.*, *10*, 313.

Houston, J., and A. J. Hartley (2003), The Central Andean west-slope rainshadow and its potential contribution to the origin of hyper-aridity in the Atacama Desert, *Int. J. Climatol.*, *23*, 1453–1464.

Insel, N., C. J. Poulsen, T. A. Ehlers, and C. Sturm (2012), Response of meteoric $\delta^{18}O$ to surface uplift—Implications for Cenozoic Andean Plateau growth, *Earth Planet. Sci. Lett.*, *317–318*, 262–272.

Jordan, T. E., P. L. Nester, N. Blanco, G. D. Hoke, F. Dávila, and A. J. Tomlinson (2010), Uplift of the Altiplano-Puna plateau: A view from the west, *Tectonics*, *29*, TC5007, doi:10.1029/2010TC002661.

Jordan, T. E., N. E. Kirk-Lawlor, N. Blanco, J. A. Rech, and N. J. Cosentino (2014), Landscape modification in response to repeated onset of hyperarid paleoclimate states since 14 Ma, Atacama Desert, Chile, *Geol. Soc. Am. Bull.*, *126*, B30978–B30971.

Kahle, M., M. Kleber, and R. Jahn (2002), Review of XRD-based quantitative analyses of clay minerals in soils: The suitability of mineral intensity factors, *Geoderma*, *109*(3–4), 191–205.

Kirk-Lawlor, N. E., T. E. Jordan, J. A. Rech, and S. B. Lehmann (2013), Late Miocene to Early Pliocene paleohydrology and landscape evolution of northern Chile, 19 to 20°S, *Palaeogeogr. Palaeoclimatol. Palaeoecol.*, *387*, 76–90.

Marquardt, C., J. A. Naranjo, and A. Lavenu (2006), Efectos geológicos del sismo del 13 de junio 2005, región de Tarapacá, *XI Congr. Geol. Chileno*, *2*, 435–438.

Marquet, P. A., C. M. Santoro, C. Latorre, V. G. Standen, S. R. Abades, M. M. Rivadeneira, B. Arriaza, and M. E. Hochberg (2012), Emergence of social complexity among coastal hunter-gatherers in the Atacama Desert of northern Chile, *Proc. Natl. Acad. Sci. U. S. A.*, *109*(37), 14754–14760.

Miller, K. G., M. A. Kominz, J. V. Browning, J. D. Wright, G. S. Mountain, M. E. Katz, P. J. Sugarman, B. S. Cramer, N. Christie-Blick, and S. F. Pekar (2005), The Phanerozoic record of global sea-level change, *Science*, *310*(5752), 1293.

Mintz, Y., and G. K. Walker (1992), Global fields of soil moisture and land surface evapotranspiration derived from observed precipitation and surface air temperature, *J. Appl. Meteorol.*, *32*, 1305–1334.

Moore, D. M., and R. C. Reynolds (1997), *X-Ray Diffraction and the Identification and Analysis of Clay Minerals*, Oxford Univ. Press, Oxford, N. Y.

Morell, K. D., D. M. Fisher, T. W. Gardner, P. La Femina, D. Davidson, and A. Teletzke (2011), Quaternary outer fore-arc deformation and uplift inboard of the Panama Triple Junction, Burica Peninsula, *J. Geophys. Res.*, *116*, B05402, doi:10.1029/2010JB007979.

Mortlock, R. A., and P. N. Froelich (1989), A simple method for the rapid determination of biogenic opal in pelagic marine sediments, *Deep Sea Res., Part A*, *36*(9), 1415–1426.

Nester, P. L., E. M. Gayo, C. Latorre, T. E. Jordan, and N. Blanco (2007), Perennial stream discharge in the hyperarid Atacama Desert of northern Chile during the latest Pleistocene: Proceedings of the National Academy of Science, vol. 104, pp. 19724–19729, doi:10.1073/pnas.0705373104.

Orellana Cortés, H. H. (2010), Aspectos geodinámicos del desierto costero de Atacama, sector Alto Patache (Oasis de Niebla) y Bajo Patache, MS thesis, Univ. de Chile, Santiago.

Quade, J., J. A. Rech, J. L. Betancourt, C. Latorre, B. Quade, K. Aasen Rylander, and T. Fisher (2008), Paleowetlands and regional climate change in the central Atacama Desert, northern Chile, *Quat. Res.*, *69*, 343–360.

Rech, J. A., J. Quade, and W. S. Hart (2003), Isotopic evidence for the source of Ca and S in soil gypsum, anhydrite and calcite in the Atacama Desert, Chile, *Geochim. Cosmochim. Acta*, *67*(4), 575–586.

Rech, J. A., B. S. Currie, G. Michalski, and A. M. Cowan (2006), Neogene climate change and uplift in the Atacama Desert, Chile: Geology, vol. 34, pp. 761–764, doi:10.1130/G22444.1.

Rodwell, M., and B. Hoskins (2001), Subtropical anticyclones and summer monsoons, *J. Clim.*, *14*(15), 3192–3211.

Rowley, D. B., and C. N. Garzione (2007) Stable isotope-based paleoaltimetry, *Annu. Rev. Earth Planet. Sci.*, *35*, 463–508.

Saillard, M., S. R. Hall, L. Audin, D. L. Farber, G. Hérail, J. Martinod, V. Regard, R. C. Finkel, and F. Bondoux (2009), Non-steady long-term uplift rates and Pleistocene marine terrace development along the Andean margin of Chile (31°S) inferred from ^{10}Be dating, *Earth Planet. Sci. Lett.*, *277*, 50–63.

Saillard, M., S. R. Hall, L. Audin, D. L. Farber, V. Regard, and G. Hérail (2011), Andean coastal uplift and active tectonics in southern Peru: ^{10}Be surface exposure dating of differentially uplifted marine terrace sequences (San Juan de Marcona, ∼15.4°S), *Geomorphology*, *128*(3–4), 178–190.

Sak, P. B., D. M. Fisher, T. W. Gardner, J. S. Marshall, and P. C. LaFemina (2009), Rough crust subduction, forearc kinematics, and Quaternary uplift rates, Costa Rican segment of the Middle American Trench, *GSA Bull.*, *121*(7–8), 992–1012.

Schemenauer, R. S., and P. Cereceda (1992), The quality of fog water collected for domestic and agricultural use in Chile, *J. Appl. Meteorol.*, *31*, 275–290.

Schlunegger, F., G. Zeilinger, A. Kounov, F. Kober, and B. Husser (2006), Scale of relief growth in the forearc of the Andes of Northern Chile (Arica latitude, 18°S), *Terra Nova*, *18*(3), 217–223.

Searl, A., and S. Rankin (1993), A preliminary petrographic study of the Chilean nitrates, *Geol. Mag.*, *130*(3), 319–333.

SERNAGEOMIN (2003), *Mapa Geológico de Chile: versión digital, versión 1.0* [CD-ROM]. *Servicio Nacional de Geología y Minería, Publicación Geológica Digital*, No. 4, (CD-ROM, versión 1.0), Santiago.

Sillitoe, R. H., and E. H. McKee (1996), Age of supergene oxidation and enrichment in the Chilean porphyry copper province, *Econ. Geol.*, *91*, 164–179.

Sträter, E., A. Westbeld, and O. Klemm (2010), Pollution in coastal fog at Alto Patache, northern Chile, *Environ. Sci. Pollut. Res.*, *17*, 1563–1573, doi:10.1007/s11356-010-0343-x.

Takahashi, K., and D. Battisti (2007), Processes controlling the mean tropical Pacific precipitation pattern, *J. Clim.*, *20*, 3434–3451.

United Nations Environment Program/Global Resource Information Database (1991), *Global Digital Data Sets for Land Degradation Studies: A GIS Approach*. Prepared by U. Deichmann and L. Eklundh. *GRID Case Study Ser., 4*. Nairobi.

Vargas, G., and L. Ortlieb (1998), Patrones de variaciones climáticas durante el Cuaternario tardío en la costa de la Región de Antofagasta, Chile, *Bull. l'Institut Fr. d'Etudes Andines*, *27*(3), 385–394.

Vásquez, P., and F. A. Sepúlveda (2013), Cartas Iquique y Pozo Almonte, Región de Tarapacá, *Serie Geología Básica*, Nos. 162–163, 1 mapa escala 1:100,000, Serv. Nac. de Geol. y Minería, Carta Geol. de Chile, Santiago.

Victor, P., O. Oncken, and J. Glodny (2004), Uplift of the western Altiplano plateau: Evidence from the Precordillera between 20° and 21°S (northern Chile), *Tectonics*, *23*, TC4004, doi:10.1029/2003TC001519.

Vivallo, W., and F. Henriquez (1998), Génesis común de los yacimientos estratoligados y vetiformes de cobre del Jurásico Medio a Superior en la Cordillera de la Costa, Región de Antofagasta, Chile, *Rev. Geol. Chile*, *25*, 199–228.

Wang, Y., H. Xu, and S. Xie (2004), Model simulations of marine boundary layer clouds over the southeast Pacific off South America. Part II: Sensitivity experiments, *Mon. Weather Rev.*, *132*, 2650–2668.